

## H II REGIONS IN NGC 628. II. ANALYSIS OF THE SPATIAL DISTRIBUTION

R. C. KENNICUTT AND P. W. HODGE\*

Astronomy Department, University of Washington, Seattle

Received 1975 October 16

## ABSTRACT

Analysis of the spatial distribution of 662 H II regions in the galaxy NGC 628 gives information on their radial distribution, their transverse (across-arm) distribution, their longitudinal (along-arm) distribution, and their tendency to clump along the arms. Radially, the H II regions show a peak near the center ( $r \sim 1.5$  kpc), followed by a generally level curve to  $r \sim 11$  kpc, beyond which the distribution falls off exponentially. The integrated across-arm distributions for the two main arms have half-widths of about 2.8 kpc. Both arms show a surprisingly uniform along-arm density, but differ from each other by a large systematic difference. Statistical tests for non-randomness ("clumping" of certain sorts) include the use of power spectrum analysis and filtered autocorrelation functions. No significant tendency for clumping on the scales tested is found. H II region distributions along various uniform galactic radii do not clearly agree with theoretical predictions, though statistics are poor.

*Subject headings:* galaxies: individual — galaxies: structure — nebulae: general

## I. INTRODUCTION

H II regions have long been recognized as delineators of spiral structure in galaxies and as important indicators of other large-scale galactic properties. Recently theories of spiral structure (e.g., see reviews by Wielen 1974 and Roberts 1974) and of galaxy evolution (Talbot and Arnett 1975) have enabled detailed predictions of H II region distributions to be formulated. For that reason we have undertaken an investigation of the spatial distribution properties of the H II regions in one rich galaxy for which a wealth of data exists, the Sc galaxy NGC 628 (M74). A map and catalog of H II regions in this galaxy has been published (Hodge 1976, hereafter referred to as Paper I). In this paper we use the data published there on the positions of the H II regions, restricting ourselves to those recorded by the 84 inch (2.1 m) telescope. We discuss the basic techniques which were used to analyze the data in § II. In § III the radial distribution of the H II regions is shown, and the results are compared with two simple models. In §§ IV and V we discuss the details of the distribution of the H II regions in the spiral arms. Included are a description of the arm-fitting procedure, the across-arm distribution of H II regions, and the along-arm distributions. In § V we look specifically at the question of "clumping" of H II regions along the arms by analyzing both power spectra and filtered autocorrelation functions for each of the two major arms in the galaxy. Finally in the last section the results obtained are compared with theoretical predictions.

\* Visiting Astronomer, Kitt Peak National Observatory, which is operated by the Association of Universities for Research in Astronomy, Inc., under contract with the National Science Foundation.

## II. METHOD OF ANALYSIS

In order to analyze in detail the distribution properties of the H II regions in NGC 628, their Cartesian positions were recorded by the University of Washington Computer Center's digitizer, and the data punched on cards. In order to deal with the positions of the H II regions in the plane of NGC 628 we mathematically rectified the galaxy by the proper amount. Rather than using previously published estimates of the inclination angle and position angle for NGC 628, we first devised an independent method of rectification. First the unrectified H II region positions in the most uniform spiral arm (arm 2 in Paper I and hereafter) were fitted by least squares to a logarithmic spiral. It was found that the H II regions deviated systematically from the fit, approximately sinusoidally with a period of  $360^\circ$ , as one would expect if the galaxy were inclined to the line of sight. We thus derived the approximate inclination and position angle of the galaxy from the amplitude and phase of the deviation, respectively. This resulted in an empirically determined value of  $w = 35^\circ \pm 3^\circ$  (estimated error) for the inclination and  $\text{p.a.} = -2^\circ \pm 5^\circ$  for the position angle. This agrees well with values determined independently with different methods by Danver (1942) ( $w = 34.9^\circ$ ,  $\text{p.a.} = 0.4^\circ$ ) and Roberts (1969) ( $w = 35^\circ$ ). It should be noted that this method of determining the orientation of a spiral galaxy is dependent on the regularity and richness of the spiral arms used as well as the logarithmic spiral assumption, and thus is somewhat limited in its applicability.

Once the orientation of the galaxy had been determined, the coordinates of 662 H II regions were transformed to the plane of NGC 628, and both the Cartesian and polar coordinates were determined. The spatial positions in kiloparsecs were computed using

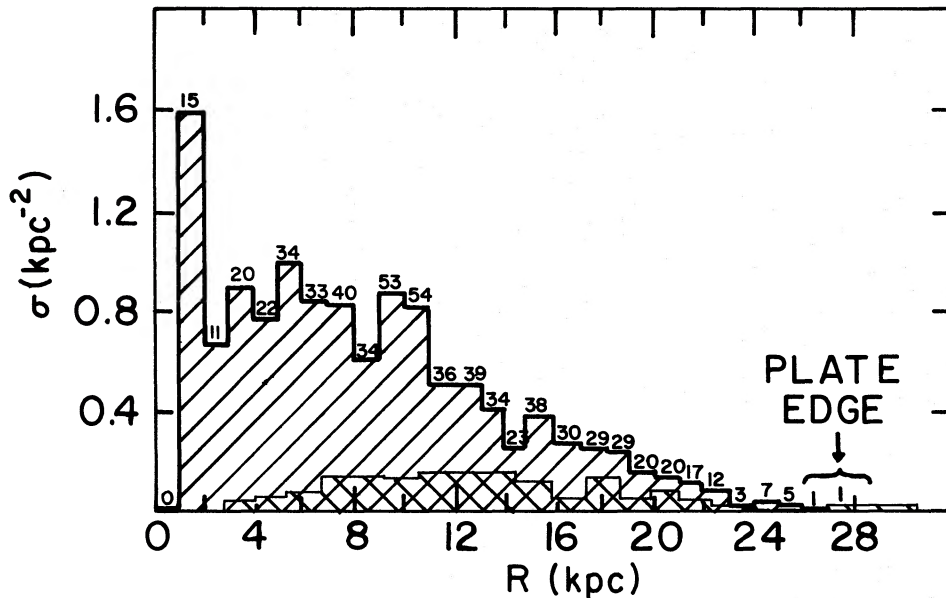


FIG. 1.—Radial distribution ( $\text{H II}$  regions  $\text{kpc}^{-2}$ ) in the plane of NGC 628. The small number above each bin denotes the actual number of  $\text{H II}$  regions in each 1 kpc annulus. The crosshatched area represents the distribution from less deep 48 inch Schmidt plates.

the Sandage-Tammann (1975) distance to NGC 628 of 18.2 Mpc.

The spiral-arm fitting procedure is described in § IV.

### III. RADIAL DISTRIBUTION

The variation of number density of  $\text{H II}$  regions as a function of distance from the center of NGC 628 is depicted in Figure 1. The distribution is similar to results found earlier for other late-type galaxies. There is a sharp rise near the center from a central minimum. The central peak is at  $r \sim 1.5$  kpc and is followed by a generally level curve to  $r \sim 11$  kpc, beyond which the curve falls off more steeply. One somewhat unexpected result was the large number of  $\text{H II}$  regions still present within 1–2 kpc of the nucleus; earlier work had indicated a lack of observable  $\text{H II}$  regions inside  $\sim 3$  kpc, as depicted by the thin line in Figure 1, from the earlier study (Hodge 1969). The difference is apparently due, at least in part, to the fact that the  $\text{H II}$  regions that are abundant within 4 kpc are mostly small faint objects that are beyond the threshold of the earlier survey.

The large number of nebulae recorded gives us good enough statistics to enable us to compare the observed radial drop in density with simple model predictions. Figure 2 shows the observed density distribution with the density coordinate plotted logarithmically. The error bars represent formal  $\sqrt{N}$  Poisson standard deviations. As can be seen in the figure, the distribution lies roughly on a straight line, consistent with an exponential density drop outside of  $\sim 12$  kpc, as one would expect if the  $\text{H II}$  region density were tied to local mean matter density. The two outermost points lie significantly below this line, but these are beginning

to be affected by the limits of the edge of the plate to which the analyzed data were restricted.

Because of the surprising uniformity of density along the arms found in § IV, we have compared these data with the predicted behavior of the distributions if the density were to fall off as  $1/r$ , as would be the case for a logarithmic spiral pattern with all  $\text{H II}$  regions contained in the spiral arms and with a uniform number density along the arms. The agreement is poor, a fact that can be attributed to the presence of many interarm  $\text{H II}$  regions (48% of them lie outside the main arms as defined below) and to the fact that

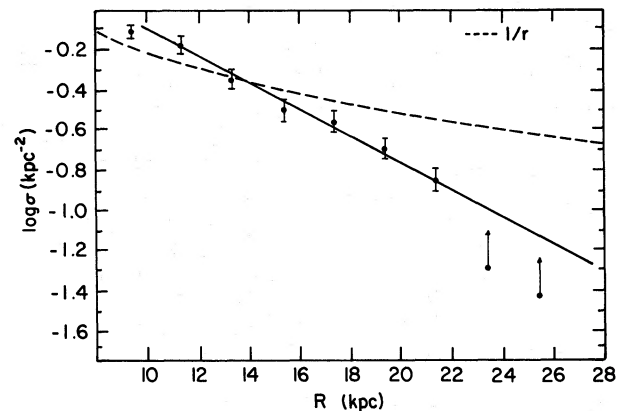


FIG. 2.—Logarithmic plot of the radial distribution. The solid line represents the best exponential fit. The dashed line represents a  $1/r$  falloff, arbitrarily fitted at 14 kpc. The last two points are near the edge of the plate, where the sample is incomplete.

TABLE 1  
H II REGIONS IN THE ARMS

| Region             | No. H II Regions Measured* | Radial Distance of Innermost H II Region (kpc) | Radial Distance of Outermost H II Region (kpc)* | Least-Squares-Fit Pitch Angle |
|--------------------|----------------------------|--|---|-------------------------------|
| Arm 1.....         | 146                        | 1.9  | 26.2  | 78°8                          |
| Arm 2.....         | 200                        | 1.6  | 17.9  | 76°2                          |
| Entire galaxy..... | 662                        | 1.6  | 27.1  | ...                           |

\* Data based on 2.1 m telescope plates only.

the two main arms extend only out to 18 kpc in clearly distinguishable form.

#### IV. DISTRIBUTION IN SPIRAL ARMS

The large sample of H II regions in this study allows a detailed look at the distribution of H II regions within the spiral arms themselves. In this section we consider the across-arm distributions and along-arm distributions.

##### a) Method of Analysis

NGC 628 was chosen as the subject for our detailed study because it possesses a spiral arm (arm 2) that fulfills the two criteria of reasonable regularity and continuity. Such arms are relatively rare. It also has an arm that is more typically somewhat irregular and discontinuous (arm 1). Table 1 summarizes some of the properties of these arms. The numbering convention follows from Paper I.

The problem of determining arm membership was solved in a somewhat arbitrary way by drawing lines parallel to the arms on either side, with a mean spacing of about  $\pm 3$  kpc. This spacing was somewhat tighter in the central areas, where the arms are closer together. These boundaries included all H II regions in the inner part of the galaxy, but omitted many H II regions beyond  $r \sim 10$  kpc, where arm branching and considerable numbers of interarm H II regions exist. Arm 2 is the more uniform and continuous of the two. Arm 1 is moderately distorted by various effects, especially at the outer end where branching occurs. The conspicuous distorting group of H II regions at  $r = 11$  kpc in the north is at the intersection of two features described by Hayward (1964) as remnants of explosive events.

Since it was our goal to study the distribution of H II regions both across and along the spiral arms, a mean spiral curve had to be defined. This was done by fitting the rectified positions of the H II regions in each of the arms by least squares to a logarithmic spiral. The justification for the logarithmic spiral form was based on the work of Danver (1942) and the discussion by de Vaucouleurs (1959). The fit for the 200 H II regions in arm 2 was excellent, as shown above; derived inclination and position angles agree well with those determined by Danver using different methods.

Arm 1 does not fit as well to a logarithmic spiral, but a reasonable fit was possible, and the pitch angles of the best fit for both arms agreed well (Table 1).

##### b) Across-Arm Distribution

The deviation of each H II region, measured perpendicular to the mean spiral, was computed to give an integrated profile of H II region density across each of the arms, as shown in Figure 3. The profile has a nearly symmetrical and approximately Gaussian character with a half-width of  $\sim 2.8$  kpc. It should be mentioned that the edges of the arms were somewhat arbitrarily established, as described above, and so the tails of the Gaussian-like distributions are artificially truncated at  $\Delta X \sim \pm 3$  kpc.

It is important to ascertain, however, whether the across-arm profiles were contaminated by deviations of the true arm from the fitted logarithmic spiral. This

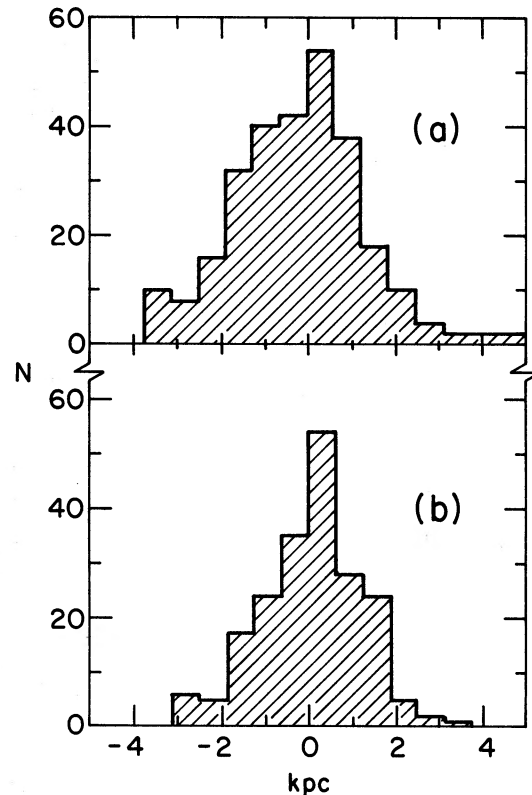


FIG. 3.—Distribution of H II regions across the arms. (a) Arm 1, (b) arm 2. Negative displacements are inside the least-squares-fit logarithmic spiral; positive displacements are outside it.

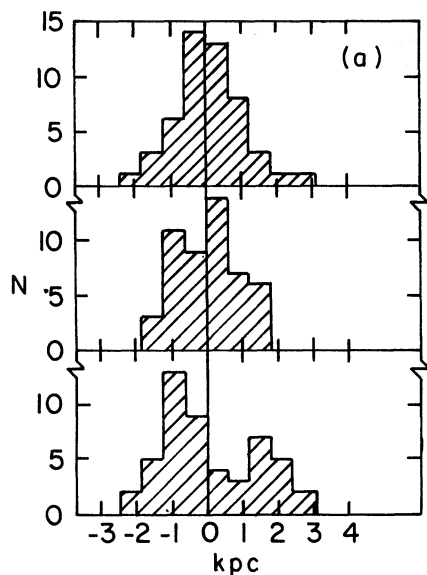


FIG. 4a

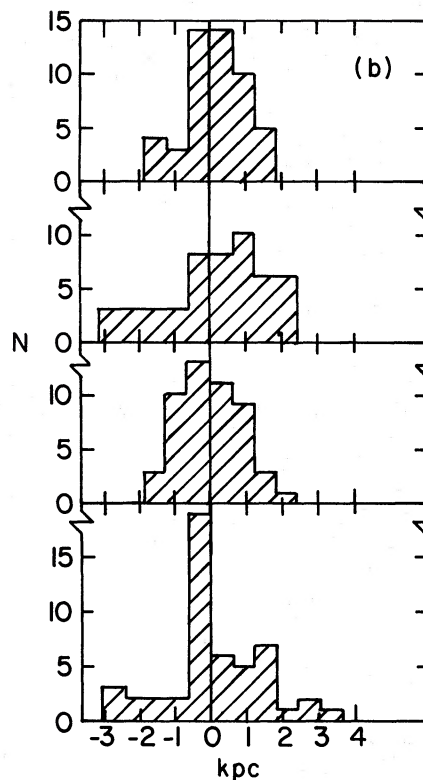


FIG. 4b

FIG. 4.—Across-arm distribution for individually fitted arm segments. (a) Arm 1, (b) arm 2. (See text for explanation of the difference between Fig. 3 and Fig. 4.)

was tested by dividing each arm into segments of 50 H II regions each, three for arm 1 and four for arm 2. Then each segment was individually fitted to a least-squares logarithmic spiral, thus defining a more local reference line for defining transverse displacements from the arm. The resulting across-arm distributions for these individually fitted segments appear in Figure 4. These indicate that the asymmetry shown in Figure 3 comes from the convolution of the least-squares fit onto the true across-arm distribution. The segments are a set of Gaussians, some symmetric, some slightly asymmetric, which are displaced with respect to each other and with respect to the overall least-squares fit. In constructing the integrated across-arm distribution, these displaced Gaussians are superposed, and the superposition of displaced symmetric distributions apparently accounts for the asymmetry observed in the overall distribution.

### c) Along-Arm Distribution

To determine whether the H II region density along a spiral arm varies systematically, in terms of a large-scale gradient in density along an arm, we measured the displacement of each H II region along the spiral arm. For a logarithmic spiral of the form

$$r = r_0 e^{k\phi},$$

where  $k$  is the tangent of the pitch angle  $\mu$ , the longitudinal displacement along the spiral, denoted as  $S$ , is

$$S = \frac{(1 + k^2)^{1/2}}{k} r_0 (e^{k\phi} - 1),$$

where  $S$  is defined as zero at  $\phi = 0$ . The projected longitudinal position of each H II region on the mean spiral was computed by this equation, and a histogram of H II region density versus displacement along the mean spiral was made for each arm (Figs. 5 and 6). Two rather surprising results emerge. First, it is found that the large-scale density of H II regions remains remarkably uniform throughout the total lengths of the arms. The degree to which this uniformity exists can be seen more easily in Table 2, where the arms are divided into quarters (lengthwise along the arm) and the numbers of H II regions per quarter compared. It can be seen that there is a small gradient in density as one proceeds outward along the arms, but the densities are still remarkably uniform.

The second surprising result is that, although the longitudinal densities of H II regions in each of the two arms is nearly uniform for each, the mean value of the density for the two arms differs by a factor of 1.8. This is observationally and statistically significant, and thus a real physical difference must exist for the two arms.

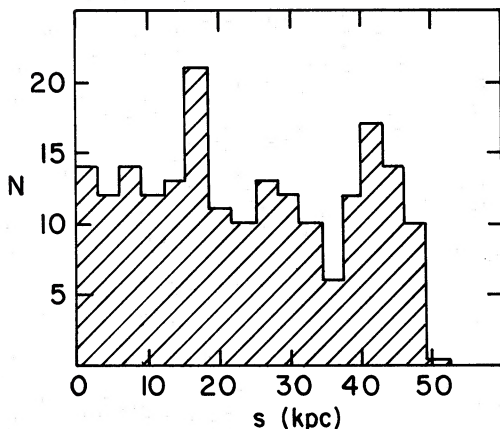


FIG. 5.—Longitudinal distribution of H II regions along arm 2. The drop at 50 kpc coincides with the edge of the plate.

Arm 2, with the larger density, is also the arm with the most perfect and uniform shape. A simple explanation on the basis of a disruption of the outer parts of arm 1 cannot hold, as the difference in H II density extends right up to the center. Apparently some unidentified physical parameter connected with arm 1 is the cause both of its lower density and its more disturbed structure.

#### V. TESTS FOR CLUSTERING

This section deals with the question of whether there exist systematic small-scale structures in the H II region distribution, relating to the question of whether the spiral-arm process tends to form the H II regions in clumps of some characteristic size. The large sample of nebulae available to us in the two major arms of NGC 628 has enabled us mathematically to test for clustering by computing one-dimensional power spectra and autocovariance functions for each of the arms. Each test is described separately.

##### a) Power Spectrum Analysis

Ideally the most direct test for clustering of the H II regions would be to compute the two-dimensional Fourier transform and the resulting power spectrum coefficients for the entire density distribution of the galaxy. However, the resultant power spectrum would

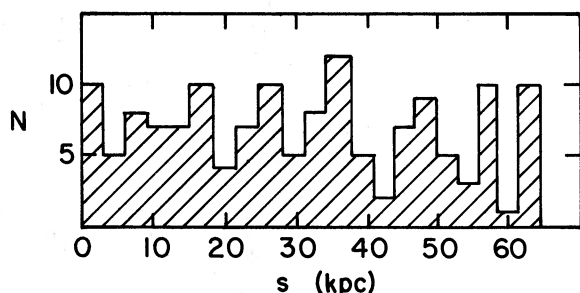


FIG. 6.—Longitudinal distribution of the H II regions along arm 1.

TABLE 2  
NUMBER OF H II REGIONS IN EACH QUARTER-ARM

| Quarter-Arm* | Arm 1<br>(64 kpc length) | Arm 2<br>(55 kpc length) | Total |
|--------------|--------------------------|--------------------------|-------|
| 1.....       | 39                       | 56                       | 95    |
| 2.....       | 38                       | 51                       | 89    |
| 3.....       | 45                       | 44                       | 89    |
| 4.....       | 34                       | 49                       | 83    |

\* First innermost.

reflect not only the spectrum of any clustering present but also features due to the spiral structure itself. These features would contaminate the spectrum at all wavelengths down to those of order of the arm width ( $\sim 1-3$  kpc), so that such a resultant power spectrum would be uninterpretable.

To avoid these problems, we chose instead to compute the power spectrum of the one-dimensional distribution of H II regions along each spiral arm. The projected longitudinal positions of all H II regions along an arm formed the one-dimensional set of points to be analyzed. Techniques for computing power spectra of sets of discrete points have been developed and applied recently by, for example, Yü and Peebles (1969), Burbidge and O'Dell (1972), and Lake and Roeder (1972). Our discussion will parallel that of Lake and Roeder. The method of analysis can be summarized as follows:

- 1) We started with the set of  $N$  H II region positions,  $S_i$ , along the arm.
- 2) The  $N$  linear positions,  $S_i$ , were converted to the interval  $0-2\pi$ , thus forming the set of points:

$$\bar{S}_i = \frac{2\pi}{L} S_i,$$

where  $L$  is the total length of the arm.

- 3) The complex Fourier coefficients for each frequency  $n$  were computed using a Fourier transform, simplified for the discrete point set,

$$Z_n = N^{-1/2} \sum_{i=1}^N \exp(in\bar{S}_i)$$

or

$$Z_n = N^{-1/2} \sum_{i=1}^N (\cos n\bar{S}_i + i \sin n\bar{S}_i).$$

- 4) The power spectrum is the set of  $|Z_n|^2$ .

5) The significance of each coefficient of the power spectrum was evaluated statistically as described in Lake and Roeder (1972), where more details can be found.

The probability that at least one coefficient  $Z_n$  of a power spectrum of  $m$  total coefficients will exceed a given level  $\chi_0$  is

$$\text{Prob. } (>\chi_0) = 1 - [1 - \exp(-\chi_0)]^m.$$

We can thus define a confidence level for a given power spectrum.

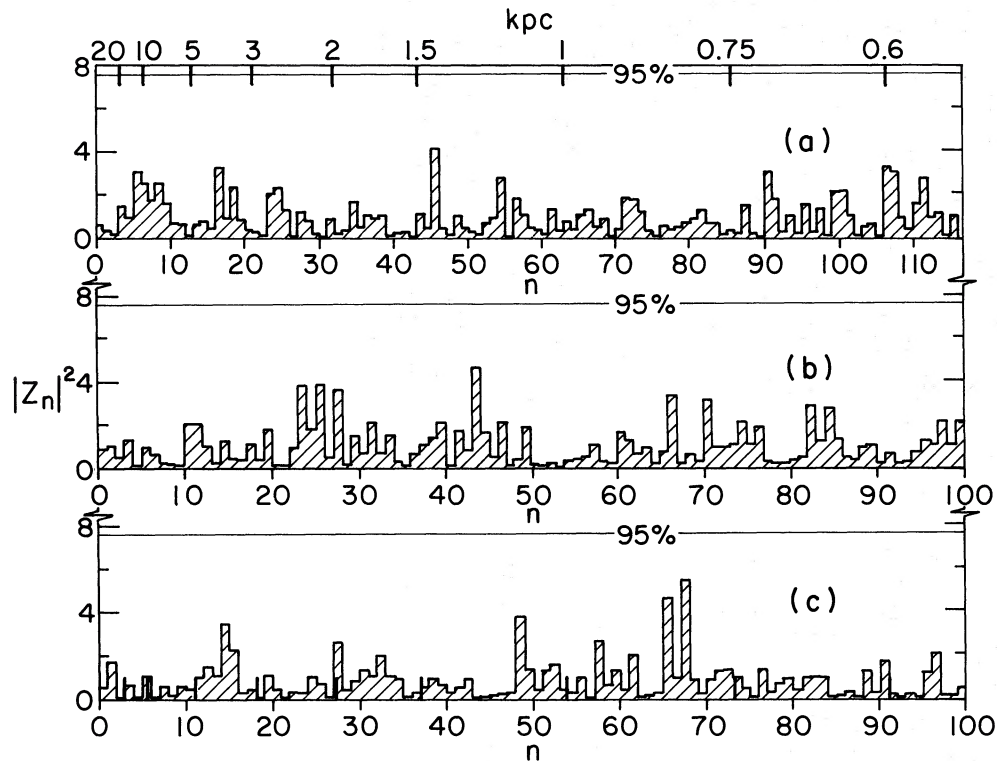


FIG. 7.—Computed power spectra. The dashed line represents the 95 percent confidence level for any one coefficient. (a) Arm 1, (b) arm 2, (c) 200 randomly distributed points. The scale is normalized to that of arm 2.

Figure 7 shows the power spectrum obtained for each of the arms in NGC 628. The dotted line represents the 95 percent confidence level. The abscissa is labeled both in terms of  $n$ , the frequency (the fraction of the total arm length), and in terms of the wavelength  $\lambda$  in kiloparsecs. Since the two arms are of unequal length, the relationship between  $n$  and  $\lambda$  for each is different.

In Figure 7 the horizontal scales have been matched in wavelength  $\lambda$ . We also show in Figure 7 the power spectrum of a set of 200 points randomly distributed in the interval  $0-2\pi$ . Though the arm distributions do not appear to be random, there exist no periodicities at the 95 percent confidence level. The only candidate is a very narrow peak at  $\sim 1$  kpc, which shows up for

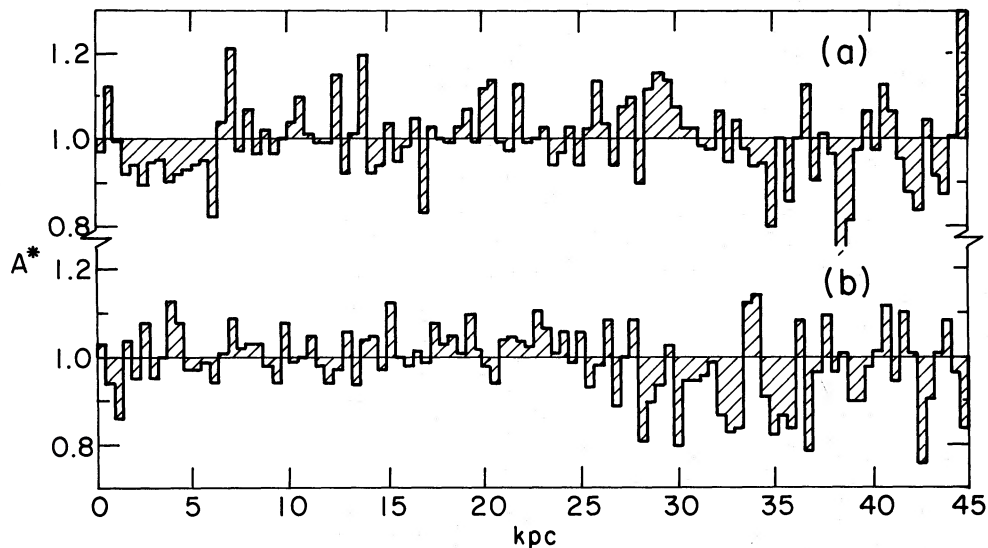


FIG. 8.—Filtered autocorrelation functions  $0 \leq D \leq 45$  kpc; (a), (b) as in Fig. 7

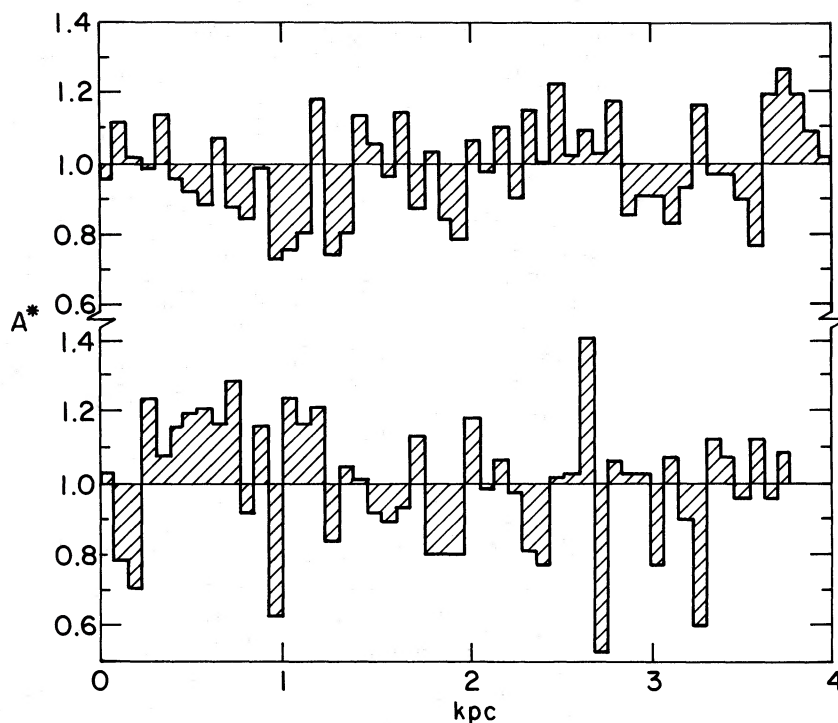


FIG. 9.—Filtered autocorrelation functions  $0 \leq D \leq 4$  kpc; (a), (b) as in Fig. 7

both arms but which is not statistically significant. Of course, the power spectrum is primarily a test for periodicities, not clustering per se, and we cannot immediately conclude that clustering is marginal or does not exist (see below).

#### b) Filtered Autocorrelation Function

In order to gain additional insight into the question of clustering in the arms, we computed the spectrum of along-arm distances of each H II region from every other H II region. If the H II regions tend to fall in clusters of order of size  $L$ , we would expect to find an excess of neighbors at distances  $L$  or less, and a depletion of neighbors slightly greater than  $L$ . This function when normalized is simply the autocorrelation function, and is the Fourier transform of the power spectrum. Its use as well as that of the power spectrum is discussed extensively by Blackman and Tukey (1958).

Before plotting the resultant autocorrelation function, one modification was made. The function contained a linearly decreasing component, caused by the finite length of the arm. The component is easily removed, and the resulting filtered autocorrelation functions are shown in Figures 8 and 9. Figure 8 depicts the large-scale ( $0 \leq D \leq 45$  kpc) character of the function, while Figure 9 concentrates on small separations of primary interest,  $D < 4$  kpc. The increasing scatter for large distances results from the decreasing number of H II regions at large separations, with the resultant degradation in statistics.

Little systematic behavior in the function can be seen, although a few striking features appear in either arm 1 or arm 2 alone. For example, Figure 8 shows a rather marked deficiency of H II regions separated by  $\sim 1-6$  kpc in arm 1, a feature which, however, is entirely absent in arm 2, which in fact exhibits a slight excess of spacings in this range. Similar discordant behavior between the two arms can be seen on smaller scales in Figure 9, especially in the range 0–1.5 kpc. It is doubtful that statistical error alone can account fully for the individual features mentioned above. Each point (bin) in the range 0–10 kpc represents typically  $\sim 300$  H II region separations in arm 2 ( $\sim 150$  for arm 1) since the total number of distance points for  $N$  H II regions is  $N^2/2$ . However, the lack of generality of the features indicates that they represent the peculiarities in the substructure of each individual arm, not the general scale of any clumping that could be part of the “grand design” of spiral arm formation.

#### c) Conclusions

The H II regions in the two major arms of NGC 628 show no strong features in either their power spectra or the autocorrelation functions. This does not, however, mean that clustering is necessarily completely absent. Strictly speaking, the power spectrum tests only for periodicity, not for clustering. If the H II regions were organized into clusters a few kiloparsecs in size and separated by many kiloparsecs along the arms, these features would show up in both the power spectrum and the autocorrelation spectrum, especially

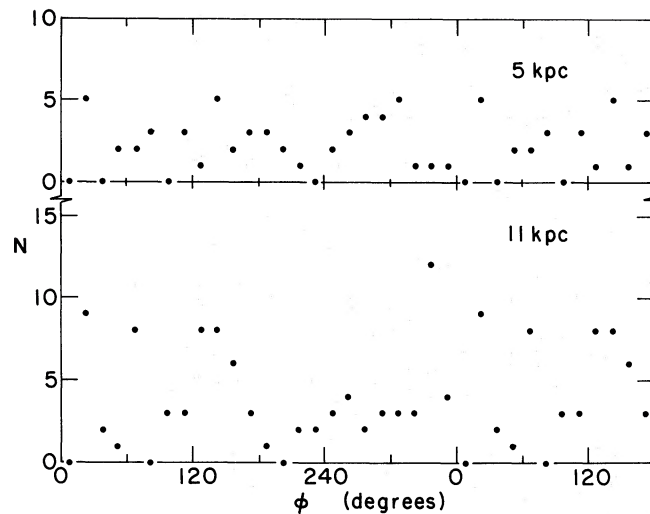


FIG. 10.—The distribution of H II regions in circular rings 2 kpc wide, with data combined for every 15° of longitude. Two examples, at 5 and 11 kpc, are shown.

in the latter. Our analysis of both test distributions and of other galaxies in which obvious large-scale structures in the arms were present have reinforced this conclusion. Thus we conclude that the lack of major features in the power spectra and autocorrelation spectra exclude the possibility of the existence of discrete, uniform-sized, and well-separated clusterings of H II regions in NGC 628. However, our tests are in all likelihood insensitive to (a) clusterings of size and/or spacing less than  $\sim 1$  kpc, where a peak in the power spectrum, if present, would be spread over tens of coefficients in the spectrum; (b) uniform-sized clusterings with separations that are random and of the same order as the size of the clusterings; and (c) clusterings of randomly distributed sizes with random separations, which would escape detection if there were enough of them for their individual effects on the power spectrum and autocorrelation to cancel. Of course, resolution or merging problems mean that very close physical associations of H II regions (with distances much less than 1 kpc) would be difficult to detect.

#### VI. CIRCULAR PROFILES

One further comparison with theoretical models is possible for the present data. Because the majority of disk stars have nearly circular orbits in a galaxy, we

can examine circular profiles of a galaxy to sample the history of events that occur at a particular radius during and between encounters with the hypothesized density wave. For example, the results of Roberts (1974) suggest that there would be a sudden increase in gas density at the shock front, where the H II regions and newly born stars should make their appearance. As one continues past the leading edge of the density wave, the gas density more gradually declines to an interarm, nearly level minimum. Schweizer (1976) has made an interesting comparison of models such as this with surface photometry of spiral galaxies and has found a disappointing lack of agreement. Similarly, we also do not detect a clear pattern like that predicted, as shown by the two examples of H II region circular profiles given in Figure 10. While one can discern a crude double sine wave pattern, the data do not show the sudden rise and gradual decline expected from the basic theoretical models. Statistics are poor, however, and it is probably preferable to make this particular kind of test with starlight, where spatial resolution is less limited.

We gratefully acknowledge the help of the staff of the Kitt Peak National Observatory and the support of the National Science Foundation, Astronomy Program, through grant MPS 74-15274.

#### REFERENCES

- Blackman, R. B., and Tukey, J. W. 1958, *The Measurement of Power Spectra* (New York: Dover).  
 Burbidge, G. R., and O'Dell, S. L. 1972, *Ap. J.*, **178**, 583.  
 Danver, C. G. 1942, *Ann. Obs. Lund.*, No. 10.  
 de Vaucouleurs, G. 1959, *Handbuch der Physik*, Vol. 53, p. 308.  
 Hayward, R. 1964, *Pub. A.S.P.*, **76**, 35.  
 Hodge, P. W. 1969, *Ap. J.*, **155**, 417.  
 ———. 1976, *Ap. J.* (in press) (Paper I).  
 Lake, R. G., and Roeder, R. C. 1972, *J.R.A.S. Canada*, **66**, 111.  
 Roberts, M. S. 1969, *A.J.*, **74**, 859.  
 Roberts, W. W. 1974, in *Highlights of Astronomy*, Vol. 3, ed. G. Contopoulos (Dordrecht: Reidel).  
 Sandage, A. R., and Tammann, G. A. 1975, *Ap. J.*, **196**, 313.  
 Schweizer, F. 1976, *Ap. J. Suppl.*, in press.  
 Talbot, R. J., and Arnett, W. D. 1975, *Ap. J.*, **197**, 551.  
 Wielen, R. 1974, *Pub. A.S.P.*, **86**, 341.  
 Yü, J. T., and Peebles, P. J. E. 1969, *Ap. J.*, **158**, 103.

PAUL W. HODGE and R. C. KENNICUTT: Astronomy Department FM-20, Physics Bldg., University of Washington, Seattle, WA 98195